Multiphoton Excitation Provides Optical Sections from Deeper within Scattering Specimens than Confocal Imaging

Victoria E. Centonze* and John G. White*#
*Integrated Microscopy Resource and #Laboratory of Molecular Biology/Department of Anatomy, University of Wisconsin, Madison, Wisconsin 53706 USA

ABSTRACT Multiphoton excitation fluorescence imaging generates an optical section of sample by restricting fluorophore excitation to the plane of focus. High photon densities, achieved only in the focal volume of the objective, are sufficient to excite the fluorescent probe molecules by density-dependent, multiphoton excitation processes. We present comparisons of confocal with multiphoton excitation imaging of identical optical sections within a sample. These side-by-side comparisons of imaging modes demonstrate a significant advantage of multiphoton imaging; data can be obtained from deeper within biological specimens. Observations on a variety of biological samples showed that in all cases there was at least a twofold improvement in the imaging penetration depth obtained with multiphoton excitation relative to confocal imaging. The more pronounced degradation in image contrast deep within a confocally imaged sample is primarily due to scattered emission photons, which reduce the signal and increase the local background as measurements of point spread functions indicated that resolution does not significantly change with increasing depth for either mode of microscopy. Multiphoton imaging does not suffer from degradation of signal-to-background to nearly the same extent as confocal imaging because this method is insensitive to scatter of the emitted signal. Direct detection of emitted photons using an external photodetector mounted close to the objective (possible only in a multiphoton imaging system) improves system sensitivity and the utilization of scattered emission photons for imaging. We demonstrate that this technique provides yet further improvements in the capability of multiphoton excitation imaging to produce good quality images from deeper within tissue relative to confocal imaging.

INTRODUCTION

The introduction of commercial confocal microscopy in the late 1980s revolutionized fluorescence microscopy (Brakenhoff, 1985; White et al., 1987; Pawley, 1995); no longer were biologists limited to looking at thin specimens in an effort to obtain clear images of fluorescently labeled structures. Because of the ability of confocal microscopy to exclude out-of-focus information, it became possible to collect images from within a thick sample that had comparable or superior clarity to epifluorescence images of flattened or sectioned specimens. Nevertheless, confocal imaging has some limitations. Photobleaching of the fluorophore in focal planes above and below the plane being observed can be problematic as focusing on one plane can produce photobleaching in all planes, including those that have not yet been observed. In addition, when collecting a stack of images from an extended volume, the signal from deeper sections will be degraded compared with those from the surface due to scattering or absorption of the excitation and emission.

Multiphoton excitation is an optical sectioning fluorescence imaging technique first demonstrated by Denk et al. (1990) whereby fluorophore excitation is confined to the plane of focus, thereby defining the optical section. Light of longer wavelength than would normally excite the fluorophore is used to illuminate the sample. As such, excitation occurs only when multiple photons are absorbed by a fluorophore simultaneously to deliver sufficient energy for the fluorophore to reach the excited state. Multiphoton absorption events are rare at typical photon densities used for conventional epifluorescence microscopy (Denk and Svoboda, 1997). To initiate enough excitation events to be practical for imaging it is necessary to deliver a very high instantaneous photon density to the specimen. To achieve this concentration of photons, high-intensity light is delivered to the sample in a diffraction-limited volume at the focus of the objective lens. The light is pulsed (typically, 100-fs, 100-MHz repetition rate) so that even though the instantaneous light intensity is extremely high, the average power received by the sample is not excessive. As the probability of two-photon excitation is proportional to the square of the photon density, the incidence of these events falls off rapidly above and below the plane of focus (Kaiser and Garrett, 1961). In this way the excitation and thus the emission is confined to a thin optical section. Without the generation of out-of-focus fluorescence there is no need to introduce a blocking pinhole in the imaging path as in a confocal microscope. Thus, all of the signal generated by a sample can be collected by the detector and can contribute to the image (Denk, 1996; Denk et al., 1994; Denk and Svoboda, 1997; Williams et al., 1994).

We have configured an imaging system that can be easily switched between confocal and multiphoton excitation im-

Received for publication 30 December 1997 and in final form 23 June 1998.

Address reprint requests to Dr. Victoria E. Centonze, Integrated Microscopy Resource, University of Wisconsin, 159M Animal Science Building, 1675 Observatory Drive, Madison, WI 53706. Tel.: 608-263-6288; Fax: 608-265-4076; E-mail: vickie@macc.wisc.edu.

0006-3495/98/10/2015/10 $2.00

aging. In addition, we have two possible options available for multiphoton detection: either descanned where the emission is directed back through the scanhead, thus retaining the facility to introduce a pinhole for enhancing resolution, or direct detection where the emission is directed to a photomultiplier (PMT) mounted beneath the objective for increased sensitivity (Williams et al., 1994; Wokosin and White, 1997; Wokosin, Amos, and White, unpublished manuscript). Therefore, using all of the same optical components, we have been able to visualize the same optical sections within a sample with each imaging mode. In this way we have been able to evaluate directly the differences in performance between conventional confocal imaging and multiphoton excitation imaging on depth of imaging penetration in a variety of biological samples. We have also determined the reduction in contrast with increased depth in the specimen for each mode of microscopy. Finally, we have evaluated the signal-to-background ratio and point spread function of both confocal and multiphoton imaging to determine how they might change with increasing depth of imaging penetration.

MATERIAL AND METHODS

Imaging system

The all-solid-state 1047-nm Nd:YLF laser (Microlase, Strathclyde, UK) and modified MRC-600 scanhead (Bio-Rad, Hempstead, UK) are configured as described in Wokosin et al. (1996) and Wokosin and White (1997). Confocal imaging was performed with a solid-state 532-nm-doubled Nd:YAG laser (ADLAS 300) mounted on the imaging system. The system was aligned to optimize the confocal image, and the beam from the infrared laser was coaxially aligned with the visible light laser for ease of comparing conventional confocal microscopy with the infrared multiphoton excitation. An infrared source blocker was not required in the MRC-600 due to low reflectivity of the internal dielectric mirrors to 1047-nm light. For confocal imaging, the signal was directed to prism-enhanced S-20 PMTs in the scanhead, and a 1.4-mm pinhole was employed to define the optical section thickness. For multiphoton excitation imaging, the emission was either directed back into the scanhead with an 8-mm pinhole (descanned) and detected by the internal PMTs or it was directed to a standard S-20 PMT (Thorn 9828B) mounted external to the scanhead directly beneath the objective of the microscope (direct detection). A source barrier filter (Chroma, Brattleboro, VT) was used for direct detection. For each imaging mode, laser power levels were adjusted to obtain an image at the surface of the specimen with a peak intensity just below saturation. Typically, the samples were irradiated with between 2 and 8 μW of visible light for confocal imaging and with between 4 and 12 mW of 1047-nm light for multiphoton imaging. Power levels were measured at the objective using a radiometer (United Detector Technology, Hawthorne, CA, model S370) for visible wavelengths and a thermopile detector (Powermax 500A meter, Molectron Detector, Portland, OR) for 1047 nm.

Specimens

Monkey kidney fixed in 10% neutral buffered formalin was sectioned to an approximate thickness of 200 μm using a vibratome. The sections were stained with acid fucsin (0.5% in distilled water) for 30 min (courtesy of M. Tengowski and A. Kutchera, Midwest Microtech, Cross-Plains, WI) and mounted in Cytoseal 60 (Stephen Scientific, Riverdale, NJ). Cheese was stained with 0.1% rhodamine B solution for 2 min. Thick sections ($\sim$200 μm) of hamster neonatal brain (courtesy of J. Callaway and K. Kalil, University of Wisconsin, Madison) were stained with 500 μg/ml FM 4–64 (Molecular Probes, Eugene, OR) for 3 min. Bovine embryo stained with 1 μM Mitotracker rosamine (Molecular Probes; courtesy of R. Krisher and B. Bavister) for 15 min. A model sample that approximates a light-scattering sample was formulated by mixing 10 μl of a concentrated yeast suspension with 10 μl of 3% agar (w/v in water). To this mixture 10 μl of a 1:100 dilution of Nile Red latex beads (mean, 0.11 μm; Spherotech, Libertyville, IL) were added. The mixture was then cast as a slab of greater than 200 μm thickness.

Data collection

The fixed specimen was viewed with a Nikon 60×, 1.4 NA oil immersion lens. All of the other samples were in aqueous medium and were viewed with a Nikon 60× 1.2 NA water immersion lens. Use of the water immersion lens reduces aberrations due to mismatched index of refraction between the mountant and the lens immersion medium (Brenner, 1994). For comparisons of deep-sectioning performance the specimen was first imaged using confocal microscopy (532-nm excitation) using a 1.4-mm pinhole, and the same optical sections were subsequently re-imaged using descanned multiphoton microscopy (1047-nm excitation) with an 8-mm pinhole. This order was maintained to ensure that the fall-off in signal seen with conventional confocal imaging was not due to the sample having been previously photobleached during multiphoton excitation. For comparisons of deep-sectioning performance in cheese, brain tissue, and bovine embryos the multiphoton images were collected by direct detection. Images at each focal plane of the samples typically were collected as a Kalman average of three frames at a resolution of 0.27 μm/pixel.

Comparison of depth of sectioning using different modes of microscopy and detection pathways was made by imaging an XZ series of acid-fucsin-stained monkey kidney using confocal microscopy with a 1.4-mm pinhole, descanned multiphoton microscopy with an 8-mm pinhole, and direct detection multiphoton microscopy. Each line of the XZ series was collected as a Kalman average of three linescans. Between linescans the stage motor was moved 0.3 μm, resulting in a voxel dimension of 0.3 μm on each side.

Signal intensity falls off with increasing imaging penetration depth. The magnitude of the fall-off varies with the light-scattering properties of the sample and also varies, in confocal imaging, with the amount of stain in overlying structures that can absorb the incident light. The acid-fucsin-stained kidney tissue was used as a model to demonstrate the extent of signal fall-off expected from a sample using confocal microscopy with a 1.4-mm pinhole, descanned multiphoton microscopy with an 8-mm pinhole, and direct detection multiphoton microscopy. XZ sections (0.3-μm resolution) were collected from five different regions in a field of view using each imaging mode. Each of the five XZ sections were then projected into a single image in which the maximal intensity was displayed for each pixel. Projecting the images smoothed some of the considerable variation in stain intensity and structure present in the individual images. Signal intensity was then plotted versus imaging penetration depth. Each datum point of the graph represents the average pixel intensity of a 3-μm (z axis, or depth) by 230-μm (x axis, or width) area of the projection image. The data are normalized to the surface value.

Determination of the point spread functions for confocal microscopy with a 1.4-mm pinhole and for descanned (no pinhole) or direct detection multiphoton microscopy were made by optically sectioning through Nile Red subresolution beads (mean diameter, 0.11 μm; Spherotech) suspended in a yeast-agar matrix. Data sets were collected at three levels: within 10 μm of the sample surface (shallow), 30–40 μm in (middle), and 70–80 μm in (deep). At each level images were collected at 0.1-μm intervals with an XY pixel resolution of 0.1 μm through a total volume 6–10 μm. The data sets were converted in NIH-Image to a stack, and the stack was then resliced to obtain an axial profile of the bead. Intensity measurements through the bead profile were measured and plotted versus depth. The point spread function was determined by measuring the full width at half maximum of the graph. To compare the point spread function of confocal or multiphoton imaging at an increasing depth, the intensity values were normalized to the maximum and plotted versus depth.

RESULTS

Comparison of optical sectioning depth

Sequences of optical sections imaged by both confocal and multiphoton excitation at increasing depths in various tissues have been used to compare the depth of imaging performance of each imaging mode. A range of samples was selected to be representative of a wide range of biological applications.

Fixed tissue

A standard histology preparation of a monkey kidney section (~200 μm thick) is shown in Fig. 1. The section was stained with 0.5% acid fucsin for 30 min and then imaged by confocal microscopy with 2 μW of 532-nm excitation (left) or by multiphoton microscopy with 4 mW of 1047-nm excitation (right). In each case the emission was descanned back to the internal PMTs of the Bio-Rad scanhead. Images at the surface of the section, closest to the objective, showed comparable intensity as well as contrast. Although the intensity of the confocal images decreases substantially by 20 μm, scaling the pixel intensities resulted in a usable image, indicating that most of the information content is still present. Although confocal images could be acquired 40 μm into the sample, the unscaled images were dark. The image resulting from scaling the pixel intensities by a factor of 3.45 shows that there had been significant degradation in

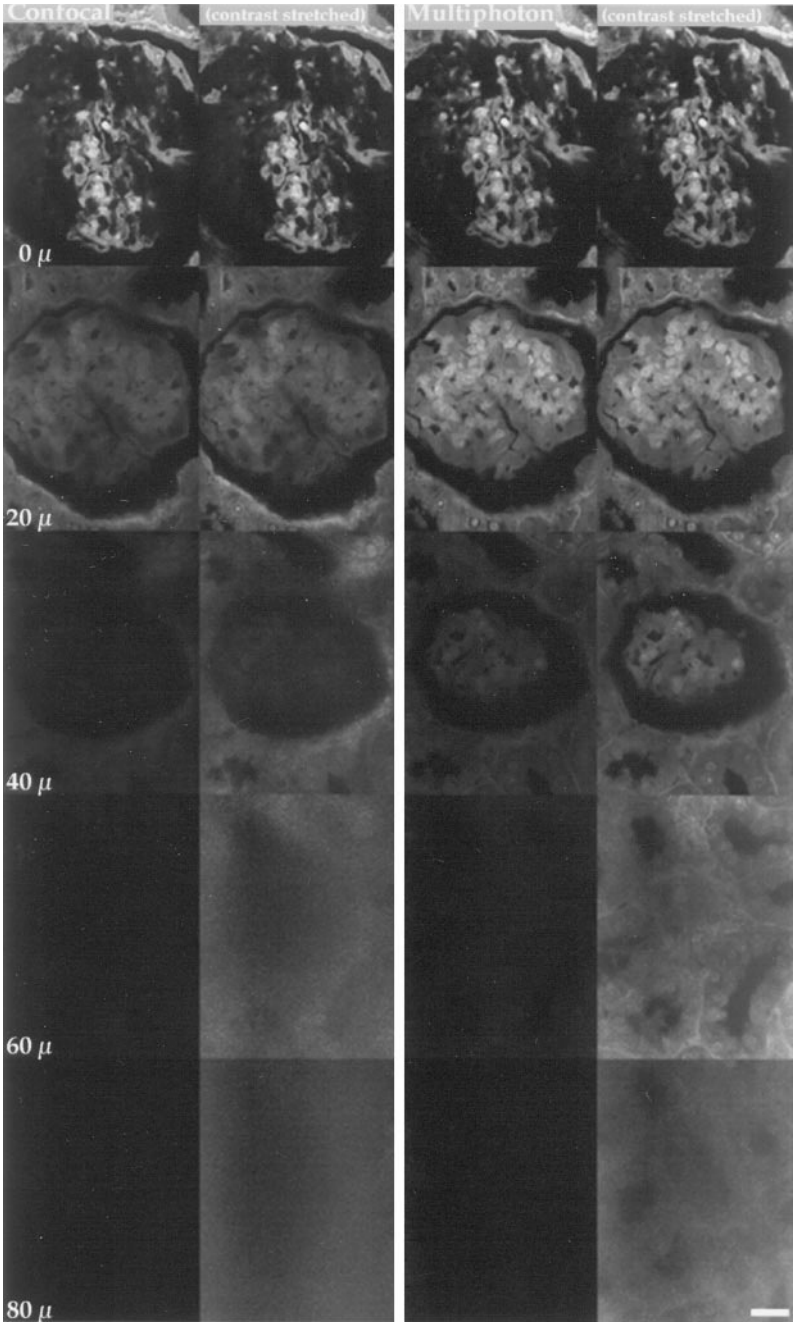

FIGURE 1 Comparison of imaging penetration depth between confocal and multiphoton microscopy. Optical sections through a glomerulus from an acid-fucsin-stained monkey kidney pathology sample imaged by confocal microscopy with 2 μW of 532-nm light (*left, columns 1 and 2*) and multiphoton microscopy with 4.3 mW of 1047-nm light (descanned; *right, columns 3 and 4*) were compared. Columns 2 and 4 represent the results of signal scaling for images collected by confocal (factors 1.00, 1.36, 3.45, 8.79, and 9.81) and multiphoton (factors 1.00, 1.00, 2.30, 7.97, and 12.14) microscopy, respectively. At the surface, the image quality and signal intensity are similar; however, at increasing depth into the sample, signal intensity and quality of the confocal image falls off more rapidly than the multiphoton image. Images were collected at a pixel resolution of 0.27 μm with a Kalman 3 collection filter. Scale bar, 20 μm.

image contrast. The fine detail has begun to be buried in the local background. However, the depth of imaging penetration attained with multiphoton imaging of the same volume was approximately twice that of confocal. The intensity of the signal resulting from multiphoton excitation was maintained at the same level up to 20 μm into the sample. Beyond this depth the signal began to diminish; however, scaling the pixel intensities of the images shows that even at 60 μm (scale factor, 7.97) into the sample sufficient information content was retained to yield a usable image although some of the fine detail begins to be lost. Scaling the images provides an appropriate way in which to represent the degradation in image content with increasing depth of imaging penetration into a sample; therefore, all subsequent figures will be displayed in this way.

Comparison of detection modes

XZ series through the monkey kidney sample (Fig. 2) shows very clearly the significant difference in depth of imaging penetration that was obtained between confocal (6 μW of 532-nm light) and multiphoton (4 mW of 1047-nm light) descanned or multiphoton direct detection. There was at least a twofold increase in imaging penetration depth for multiphoton (descanned) compared with confocal imaging. Multiphoton excitation imaging does not require the use of an interference blocking pinhole to generate an optical section. Therefore, it is not necessary to descan the emission from the fluorophore into the scanhead so as to pass through the stationary pinhole. The emission detection system can be simplified by placing the detector directly after the objective lens as described by Wokosin and White (1997). In this way more emission photons that suffer scattering may be collected. In addition, the emission follows a more direct path to the detector and does not suffer losses at each of the many optical elements in the scanhead. Consequently, the detection sensitivity of the system increases approximately threefold when using the Nikon 60× 1.4 NA oil lens (Wokosin et al., 1998) with respect to the signal collected by descanning the multiphoton emission. The increased sensitivity of detection results in better contrast in images taken at levels deeper within tissue. The difference in signal intensity, especially at greater depths within the sample, between multiphoton images collected by descanning the signal or by directly viewing the signal using an external detector shows that the limit in the ability to collect usable signal is not exclusively a limit of excitation but can be significantly affected by the limitations in sensitivity of the detection pathway. Short-path, direct detection is a more efficient mode of collecting emitted photons as more scattered emission photons may be collected and utilized for imaging. This increases the signal-to-noise ratio of the image, which in turn further increases the depth at which usable images may be obtained.

The decay in two-photon excited fluorescence inside a stained rat brain slice has been documented (Denk et al., 1994). The comparison of signal intensity fall-off for confocal and multiphoton imaging has also been documented (Wokosin et al., 1997). We have extended the analysis (Fig. 3) by comparing the fall-off in the same sample imaged by confocal (532-nm excitation), multiphoton descanned (1047-nm excitation), and multiphoton direct detection (1047-nm excitation). The graph of normalized intensity versus depth shows a precipitous fall-off with confocal compared with multiphoton imaging. Fig. 1 shows that the ability to obtain useful images degrades even more rapidly. The confocal signal became buried in background at 70 μm. Using an externally mounted detector resulted in brighter signals and enabled usable multiphoton images to be obtained well beyond 70 μm for this sample. The estimation of imaging penetration depth attained by multiphoton excitation (direct detection) with this sample was limited by the physical working distance of the objective. The vertical streaks that can be seen at the bottom of the direct detection images (Figs. 2 and 3) are a result of attempting to collect images after the objective came in contact with the coverslip.

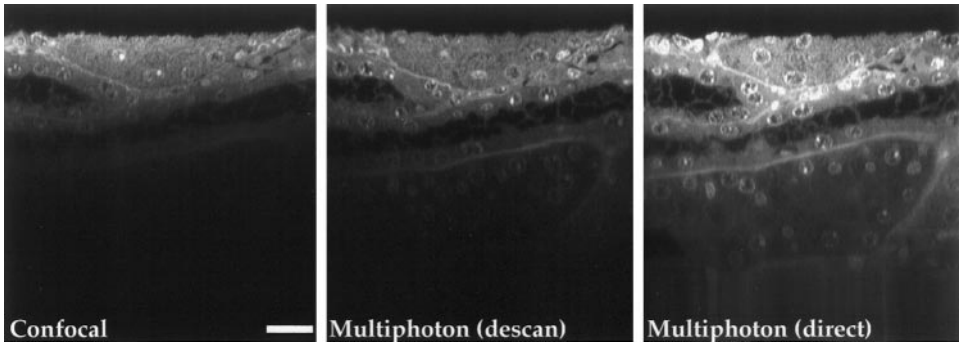

FIGURE 2 Comparison of imaging penetration depth with different imaging modes. Shown are XZ profiles through an acid-fucsin-stained monkey kidney pathology sample imaged through a depth of 140 μm with confocal (*left*), multiphoton descanned (*middle*), and multiphoton direct detection (*right*) microscopy. The imaging penetration depth with multiphoton (descanned, *middle*) relative to confocal (*left*) imaging is improved at least twofold. Direct detection (*right*) provides increased signal detection and, therefore, increased depth of imaging. XZ images were collected at 0.3-μm pixel resolution using a Kalman 3 collection filter. Scale bar, 20 μm

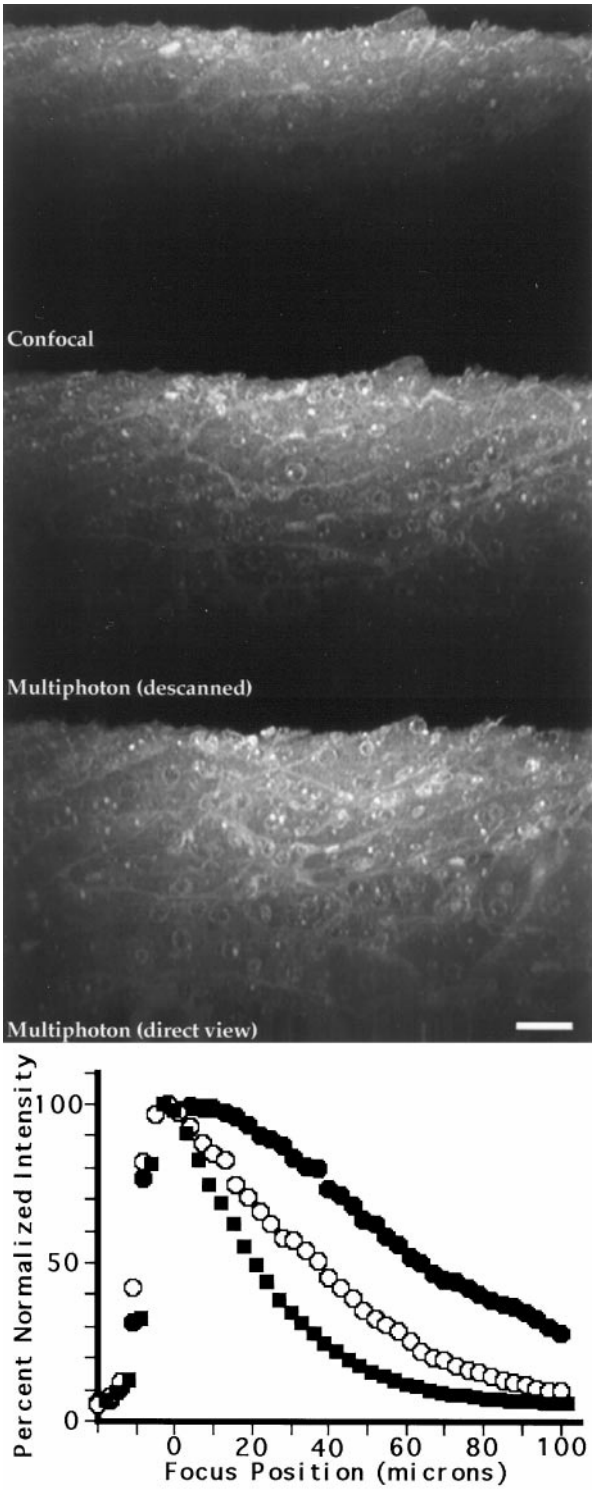

FIGURE 3 Signal intensity fall-off versus depth of imaging penetration. Projections of five XZ sections through acid-fucsin-stained monkey kidney imaged by confocal or multiphoton descanned or direct detection were measured for fluorescence intensity at increasing depth in the sample. The graph of percent-normalized intensity versus sample depth shows a rapid fall-off with confocal imaging as compared with multiphoton imaging. The fall-off for multiphoton direct detection is less rapid than for multiphoton descanned due to the improved utilization of scattered photons.

Unfixed tissue

The dairy industry uses confocal microscopy to evaluate the aqueous/lipid composition of cheese (Everett et al., 1995). The opacity of the cheese, however, limits the volume available for imaging. Cheese soaked in a solution of rhodamine dye was imaged by confocal microscopy with 6 μW of 532-nm light (Fig. 4, left) and by multiphoton imaging with 10 mW of 1047-nm light (Fig. 4, right). Once again, the imaging penetration depth with multiphoton excitation was at least twice as great as that obtained with confocal imaging.

Imaging living specimens poses significant problems. Two of these problems are reduced by the use of multiphoton microscopy; imaging penetration depth is greater and

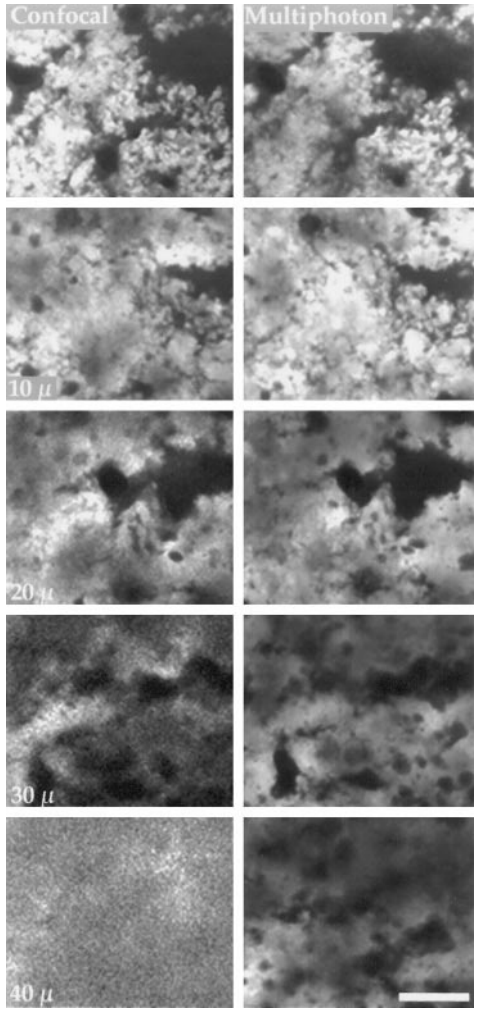

FIGURE 4 Demonstration of increased imaging penetration depth with multiphoton microscopy. A thick slice of cheese stained with 0.5% rhodamine was imaged by confocal microscopy (*left*; 6 μW of 532-nm light; signal scaling factors = 1.00, 1.00, 2.80, 4.55, and 12.75) and multiphoton microscopy (direct detection, *right*; 10 mW of 1047-nm light; signal scaling factors = 1.00, 1.00, 1.10, 1.50, and 2.90). Due to the opacity of this sample, the fall-off in signal with depth was very rapid. However, multiphoton imaging still showed at least a twofold improvement in depth of sectioning relative to confocal imaging. Images were collected at a pixel resolution of 0.27 μm with a Kalman 3 collection filter. Scale bar, 40 μm.

viability of the sample can be improved. The advantage of 1047-nm multiphoton excitation imaging for specimen viability is being addressed in another study (Squirrell et al., in preparation). Depth of imaging penetration is compromised in living specimens by light scattering due to refractive index mismatch between membranes and cytoplasmic components found in cells and embryos (i.e., membranous organelles and yolk). Brain tissue is particularly difficult to image because of the density of membranes. Fig. 5 shows a sequence of optical sections obtained at increasing depths in a slice of neonatal hamster brain that has been stained heavily (500 μg/ml) with the membrane probe FM 4–64. Confocal images obtained by excitation with 7 μW of 532-nm light (left) show significant degradation of signal beyond a depth of approximately 30 μm, yet multiphoton imaging with 10 mW of 1047-nm light continued to yield usable images at depths up to ~60–80 μm. The increased depth at which images can be obtained means that observations can be made in tissue that is removed from regions of mechanical damage from sectioning.

A living bovine embryo (~100 μm in diameter) stained with the vital mitochondria probe Mitotracker rosamine is shown in Fig. 6. Confocal imaging with 3.5 μW of 532-nm light (left) can probe to depths of ~30–40 μm yielding clear images of structures at the periphery of this spherical embryo. Structures at the center of the embryo are not visible. These images could be erroneously interpreted as indicating that mitochondrial distribution is restricted to the periphery of the embryo. Multiphoton imaging, however, gives a different result. As a result of the increased depth of imaging penetration, multiphoton imaging with 10 mW of 1047-nm light (right) can probe through the greater diameter of the embryo, thus producing a more complete picture of the distribution of mitochondria across the entire optical section. It was possible to observe the mitochondria throughout the entire volume of the sphere, including those that surround the pronuclei as seen in the midsection of the embryo.

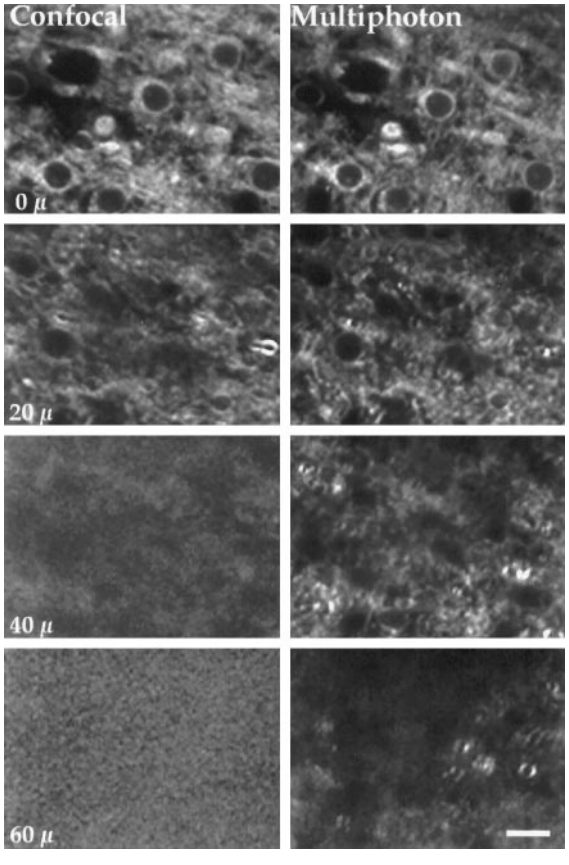

FIGURE 5 Demonstration of increased imaging penetration depth with multiphoton microscopy in an unfixed sample. A neonatal hamster brain slice stained with 500 μg/ml FM 4–64 was imaged by confocal microscopy (*left*; 7 μW of 532-nm light; signal scaling factors = 1.00, 2.00, 5.10, and 7.28) and by multiphoton excitation imaging (direct detection, *right*; 10 mW of 1047-nm light; signal scaling factors = 1.00, 1.39, 2.68, and 5.10). The confocal images become murky and the structures lose definition at depths of 20–30 μm whereas definition of structure in the multiphoton images remains at depths of at least 60 μm. Images were collected at a pixel resolution of 0.27 μm with a Kalman 3 collection filter. Scale bar, 10 μm.

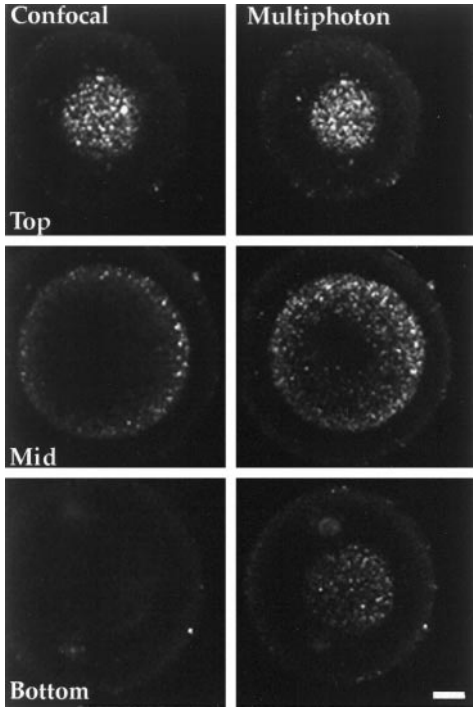

FIGURE 6 Demonstration of increased imaging penetration depth with multiphoton microscopy in a living embryo. A bovine embryo stained with Mitotracker rosamine was imaged by confocal microscopy (*left*; 3.5 μW of 532-nm light) and by multiphoton microscopy (direct detection, *right*; 10 mW of 1047-nm light). Confocal microscopy gives the erroneous impression that mitochondria are localized to the region adjacent to the cell cortex. However, the multiphoton image indicates that the mitochondrion distribution is fairly uniform throughout the cytoplasm. Images were collected at a pixel resolution of 0.27 μm with a Kalman 3 collection filter. Scale bar, 20 μm.

Investigation of signal loss

Signal-to-background

Fig. 7 shows images from the acid-fucsin-stained kidney sample at a depth of 60 μm from the surface. The laser intensities were adjusted to 550 μW of 532-nm light for confocal and 12 mW of 1047-nm light for multiphoton imaging to yield the same mean pixel intensity in each image. The confocal image is significantly inferior to the multiphoton image. A histogram representation of pixel intensities in each image shows that the pixel intensity distribution for each imaging mode is very different. The confocal image shows a narrow spread of pixel intensities whereas the multiphoton image exhibits a broad spread of pixel intensities over the full range of 255 gray levels. The confocal image is degraded for two reasons: 1) the signal is attenuated, accounting for the drop-off in high-intensity pixel values, and 2) the local background is increased. Increasing the power incident on the specimen results only in a brighter image with little contrast. A similar effect is noted when the power levels are low but the confocal pinhole is opened.

Point spread function versus depth

To investigate other possible reasons for the degradation of image quality with increasing depth we measured the point spread at increasing depths with each mode of microscopy. A light-scattering matrix of yeast, agar, and 0.11-μm Nile Red latex beads was formulated to approximate a tissue sample. Profiles of subresolution beads were analyzed at increasing depths within the sample (Fig. 8). The lateral and axial resolution for confocal microscopy with a 1.4-mm pinhole using 532-nm excitation was determined to be 0.35 μm and 0.85 μm, respectively. The lateral and axial resolution for multiphoton microscopy using 1047-nm excitation was 0.45 μm and 1.25 μm, respectively. The error for all measurements was $\pm$0.05 μm. Based on Rayleigh's criterion, the decrease in resolution with multiphoton imaging was expected, considering the excitation wavelength is approximately double that used for confocal imaging (Gu and Gan, 1996). The resolution of multiphoton imaging can be improved by employing an imaging aperture (pinhole) but with a significant loss in signal intensity (Stelzer et al., 1994; Bhawalker et al., 1996). At increasing depths into the yeast-agar matrix the point spread function of the beads did not appreciably change with increased depth for either imaging mode. This indicates that the degradation of the images in confocal microscopy is not due to a decrease in resolution but rather is due to a significant loss of signal due to scatter of the light of both excitation and emission.

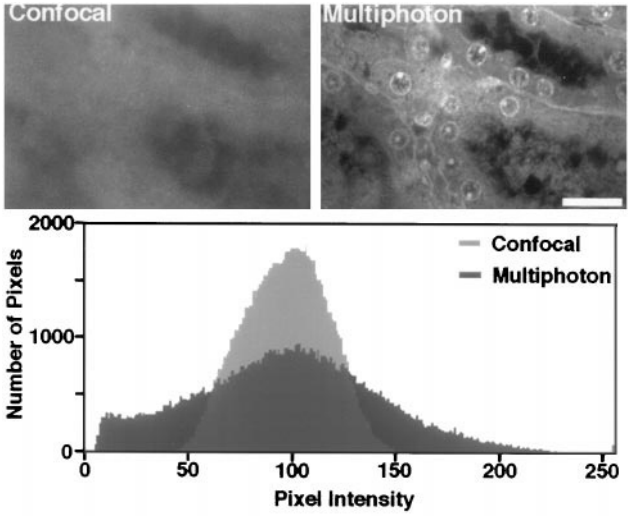

FIGURE 7 Effect of increased incident power on generation of signal. Samples of acid-fucsin-stained monkey kidney were imaged at a depth of 60 μm into the sample by confocal (550 μW of 532-nm light) and by multiphoton (12 mW of 1047-nm light) microscopy. Laser intensities were adjusted to produce the same mean number of photons per pixel. The confocal image exhibits a significantly narrower spread of pixel intensities compared to the multiphoton image indicating a lower signal to background ratio. Multiphoton imaging therefore provides a high-contrast image even at significant depths within a light-scattering sample. Images were collected at a pixel resolution of 0.27 μm with a Kalman 3 collection filter. Scale bar, 20 μm.

DISCUSSION

Reasons for improved depth of imaging with multiphoton excitation imaging

We have demonstrated that multiphoton excitation can improve the imaging penetration depth by a factor of two or more in typical biological specimens that are highly light scattering. There are several probable reasons for this result. First, light scattering is strongly wavelength dependent, being less for longer wavelengths. Therefore, scattering of source photons for multiphoton excitation imaging should be less as the wavelength is twice as long as that used for confocal imaging. Typical biological samples are complex scattering objects; however, scattering produced by small particles within the sample (Rayleigh scattering) is proportional to the inverse fourth power of the wavelength of light being scattered. Therefore, the longer wavelengths used for multiphoton excitation will be scattered much less by small particles than the visible wavelengths used for conventional confocal microscopy. As a result, the focused beam will penetrate deeper into a thick specimen so that the fluorophore at optical sections deep within a specimen can be excited (Stelzer et al., 1994; Potter et al., 1996). Second, multiphoton excitation imaging makes more efficient use of all of the signal generated from the plane of focus. Visible wavelength photons from fluorophore emission will be scattered by the specimen in the same way regardless of the mode of excitation. In the case of multiphoton imaging, out-of-focus signal is not generated so there is no need to re-image the specimen and employ an imaging aperture or pinhole to block out-of-focus interference (Williams et al., 1994; Denk et al., 1995a). Therefore, scattered photons from fluorophore emission that reach the detector can con-

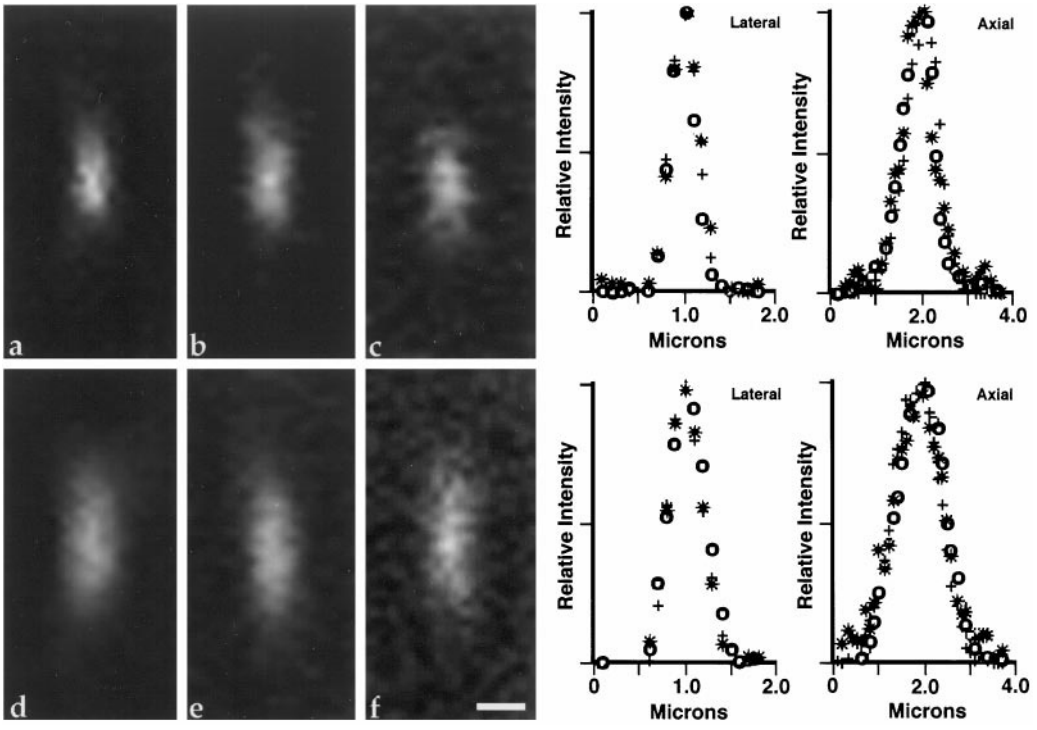

FIGURE 8 Comparisons of point spread functions between confocal (*a–c*) and multiphoton (*d–f*) microscopy. Z-series were taken of subresolution beads within a model sample at three depths: shallow, within 10 μm of the surface (*a* and *d*); middle, between 30 and 40 μm (*b* and *e*); and deep, ~70 μm (*c* and *f*). Visually, the dimensions of the point spread functions do not appear to increase with depth of imaging. This result is illustrated by graphs of normalized intensity versus axial position in the bead imaged by confocal (*upper graph*) or multiphoton (*lower graph*) microscopy at three levels within the sample (○, shallow; +, middle; *, deep). The lateral resolutions for confocal and multiphoton microscopy were 0.35 μm and 0.45 μm, respectively. The axial resolutions for the confocal and multiphoton microscopy were 0.85 μm and 1.25 μm, respectively. Images were collected at a pixel resolution of 0.1 μm with a Kalman 1 collection filter. Scale bar, 0.5 μm.

tribute to a multiphoton image. In contrast, the scattered photons from a focal volume excited by conventional confocal imaging do not contribute constructively to the final image because they are indistinguishable from photons emitted from out-of-focus regions and are for the most part blocked from reaching the detector by the confocal pinhole (Denk et al., 1994; Denk, 1996; Denk and Svoboda, 1997). Third, the visible wavelength excitation beam can be attenuated by fluorophore absorption above the plane of focus. Highly fluorescent structures in planes above the one being imaged can absorb the excitation beam thereby blocking the excitation beam from reaching fluorophore below. As a result, discrete regions under the highly fluorescent structures are shadowed. This gives rise to a mottled appearance of fluorescent structures deep within the tissue. The same effect is observed when the excitation beam must pass through a thicker portion of tissue to reach a specific focal plane such as is seen when imaging the midplane of a spherical embryo. The shadowing affect due to primary beam absorption by fluorophore is not a factor for multiphoton imaging. For two-photon excitation, the excitation rate is proportional to the square of the local beam intensity (Kaiser and Garrett, 1961). The conical geometry of the excitation beam causes the excitation intensity to vary as the inverse square of the distance from the plane of focus. Two-photon excitation will therefore vary as the inverse fourth power of the distance from the plane of focus. The result is that photon absorption is confined to a very narrow volume at the plane of focus. Therefore, the specimen above the plane of focus is essentially transparent to the excitation beam. This is only true when there is no material present in the specimen that absorbs single photons of the primary beam. Absorption of the primary beam can be a significant limitation when attempting to image pigmented material. Fourth, signal-to-background ratio of the confocal image decreases with increasing depth into a light-scattering sample. As described above, the signal from confocal excitation is decreased due to attenuation of the excitation beam and loss of emission signal due to scatter within the specimen. In addition, the local background is higher with confocal imaging as a proportion of emission photons generated and scattered in the bulk of the sample (Schmitt et al., 1994) will find their way through the confocal aperture adding to the background of the image and decreasing image contrast. Most of these scattered photons come from emission generated out of the plane of focus. As multiphoton excitation does not generate signal out of the plane of focus there are no spurious scattered photons to contribute to the background and image contrast is maintained even deep within a sample. By increasing the source power, it is possible to

compensate for attenuation of excitation at increasing depths within a sample. Although this results in a bright, crisp multiphoton image, the resulting confocal image is less than satisfactory due to degradation of the signal-to-background ratio. Axial measurements of a point sample embedded in a light-scattering medium show that the point spread function does not change appreciably with increasing depth into the sample for either confocal or multiphoton excitation imaging (Fig. 8). Therefore, loss of resolution is not a major factor in the degradation of the confocal image. The loss of contrast due to a decrease in signal-to-background ratio is the major reason for the deterioration of the confocal image.

To summarize, deterioration of confocal images relative to multiphoton images in deep optical sections is caused by 1) attenuation of excitation by fluorophore above the focal plane, 2) loss of signal due to scatter of the emission, 3) increase in background due to scattered out-of-focus emission passing through the confocal aperture, and 4) shorter excitation wavelengths that consequently suffer higher levels of scatter.

Photobleaching and Phototoxicity

In conventional confocal microscopy, while scanning each focal plane there is a bleaching octahedron within which there is uniform bleaching of the imaging probe. Therefore, photobleaching during collection of a three-dimensional data set is proportional to the superposition of the octahedrons of the individual planes (Centonze and Pawley, 1995). For regions close to the focal plane, the bleaching rate is fairly constant. Consequently, while collecting a three-dimensional data set fluorophore will be photobleached in a portion of the volume that is yet to be imaged. This can be very problematic when collecting repeated three-dimensional data sets in time-lapse (four-dimensional) imaging of living tissue. Samples imaged by multiphoton excitation imaging are not exposed to the same degree of photobleaching as fluorophore excitation, and thus photobleaching is restricted to the plane of focus (Denk et al., 1990; Stelzer et al., 1994; Denk et al., 1995a). As such, the total volume of fluorophore bleached in a sample in one confocal Z-series of 10 sections is comparable roughly to the total volume of fluorophore bleached in a multiphoton Z-series of 10 sections repeated 10 times.

Additionally, limiting the volume of excitation using multiphoton excitation also limits the concentration of phototoxic by-products of excitation such as singlet oxygens and free radicals. This may bring the rate of production of these toxic products down to levels that can be eliminated by the intrinsic scavenging mechanisms of living tissue, such as catalase and superoxide dismutase (Halliwell, 1996). Thus, physiological experiments can be performed with less perturbation due to imaging (Denk et al., 1994; Denk et al., 1995b; Yuste and Denk, 1995; Svoboda et al., 1996, 1997). A point to consider is that not all wavelengths used for multiphoton excitation imaging will be benign for live imaging (Liang et al., 1996; König et al., 1997).

CONCLUSION

The increased imaging penetration depth obtainable with multiphoton microscopy offers potential benefits to many areas of biological microscopy. For example, in pathology, rather than being limited to analysis of sections only a few microns thick it is possible to observe tissue features in situ throughout a greater volume of the tissue. In addition, these data can be collected rapidly and in digital format. This could facilitate the three-dimensional characterization of cells and nuclei for diagnostic purposes. Also, in the field of in vivo imaging multiphoton imaging has the dual advantage of being less prone to image degradation due to light scatter and of being more benign to a sample than other modes of fluorescent imaging (Denk et al., 1994; Stelzer et al., 1994; Potter et al., 1996).

This work was supported by the National Institutes of Health under Grant P41-RR00570. The authors would like to thank B. Amos, B. Bavister, J. Callaway, K. Kalil, R. Krisher, A. Kutchera and M. Tengowski for providing samples and David Wokosin for his expert technical support and critical reading of the manuscript.

REFERENCES

Bhawalker, J. D., A. Shih, S. J. Pan, W. S. Liou, J. Swiatkiewicz, B. A. Reinhardt, P. N. Prasad, and P. C. Cheng. 1996. Two-photon laser scanning fluorescence microscopy: from a fluorophore and specimen perspective. *Bioimaging*. 4:168–178.

Brakenhoff, G. J., H. T. M. Van der Voort, E. A. Van Sprosen, W. A. M. Linnemans, and N. Nanninga. 1985. Three-dimensional chromatin distribution in neuroblastoma nuclei shown by confocal scanning laser microscopy. *Nature*. 317:748–749.

Brenner, M. 1994. Imaging dynamic events in living tissue using water immersion objectives. *Am. Lab*. (April 14) 14–17.

Centonze, V. E., and J. B. Pawley. 1995. Tutorial on practical confocal microscopy and use of the confocal test specimen. *In* Handbook of Biological Confocal Microscopy. J. Pawley, editor. Plenum Press, New York. 549–569.

Denk, W. 1996. Two-photon excitation in functional biological imaging. *J. Biomed. Optics*. 1:296–304.

Denk, W., K. R. Delaney, A. L. Gelperin, D. Kleinfield, B. W. Stowbridge, D. W. Tank, and R. Yuste. 1994. Anatomical and functional imaging of neurons using 2-photon laser scanning microscopy. *J. Neurosci. Methods.* 54:151–162.

Denk, W., D. W. Piston, and W. W. Webb. 1995a. Two-photon molecular excitation in laser-scanning microscopy. *In* Handbook of Biological Confocal Microscopy. J. Pawley, editor. Plenum Press, New York. 445–458.

Denk, W., J. H. Strickler, and W. W. Webb. 1990. Two-photon laser scanning fluorescence microscopy. *Science*. 248:73–76.

Denk, W., M. Sugimori, and R. Llinas. 1995b. Two types of calcium response limited to single spines in cerebellar Purkinje cells. *Proc. Natl. Acad. Sci. U.S.A.* 92:8279–8282.

Denk, W., and K. Svoboda. 1997. Photon upmanship: why multiphoton imaging is more than a gimmick. *Neuron*. 18:351–357.

Everett, D. W., K. Ding, N. F. Olson, and S. Gunasekaran. 1995. Applications of confocal microscopy to fat globule structure in cheese. *In*

Chemistry of Structure/Function Relationships in Cheese. E. Malin and M. Tunick, editors. Plenum Press, New York. 321–330.

Gu, M., and X. S. Gan. 1996. Effect of the detector size and the fluorescence wavelength on the resolution of three- and two-photon confocal microscopy. *Bioimaging*. 4:129–137.

Halliwell, B. 1996. Mechanisms involved in the generation of free radicals. *Pathol. Biol.* 44:6–13.

Kaiser, W, and C. G. B. Garrett. 1961. Two-photon excitation in CaF_2: Eu^{2+}. *Phys. Rev. Lett.* 7:229–231.

König, K., P. T. C. So, W. W. Mantulin, and E. Gratton. 1997. Cellular response to near-infrared femtosecond laser pulses in two-photon microscopes. *Opt. Lett*. 22:135–136.

Liang, H., K. T. Vu, P. Krishnan, T. C. Trang, D. Shin, S. Kimel, and M. W. Berns. 1996. Wavelength dependence of cell cloning efficiency after optical trapping. *Biophys. J.* 70:1529–1533.

Pawley, J. B. (ed.) 1995. Handbook of Biological Confocal Microscopy. Plenum Press, New York.

Potter, S. M., C. M. Wang, P. A Garrity, and S. E. Fraser. 1996. Intravital imaging of green fluorescent protein using 2-photon laser-scanning microscopy. *Gene*. 173:25–31.

Schmitt, J. M., A. Knüttel, and M. Yadlowsky. 1994. Confocal microscopy in turbid media. *J. Opt. Soc. Am. A*. 11:2226–2235.

Stelzer, E. H. K., S. Hell, and S. Lindek. 1994. Nonlinear absorption extends confocal fluorescence microscopy into the ultra-violet regime and confines the illumination volume. *Opt. Commun.* 104:223–228.

Svoboda, K., W. Denk, D. Kleinfeld, and D. W. Tank. 1997. In vivo dendritic calcium dynamics in neocortical pyramidal neurons. *Nature*. 385:161–165.

Svoboda, K., D. W. Tank, and W. Denk. 1996. Direct measurement of coupling between dendritic spindles and shafts. *Science*. 272:716–719.

White, J. G., W. B. Amos, and M. Fordham. 1987. An evaluation of confocal versus conventional imaging of biological structures by fluorescence light microscopy. *J. Cell Biol.* 105:41–48.

Williams, R. M., D. W. Piston, and W. W. Webb. 1994. Two-photon molecular excitation provides intrinsic 3-dimensional resolution for laser-based microscopy and microphotochemistry. *FASEB*. 8:804–813.

Wokosin, D. L., V. E. Centonze, J. G. White, D. Armstrong, G. Robertson, and A. I. Ferguson. 1997. All-solid-state ultrafast lasers facilitate multiphoton excitation fluorescence imaging. *IEEE J. Select. Top. Quant. Elec.* 2:1051–1065.

Wokosin, D. L., V. E. Centonze, J. G. White, S. N. Hird, S. Sepsenwol, G. P. A. Malcolm, G. T. Maker, and A. I. Ferguson. 1996. Multiple-photon excitation imaging with an all-solid-state laser. *In* Optical Diagnostics of Living Cells and Biofluids. *Proc. SPIE*. 2678:38–49.

Wokosin, D. L., and J. G. White 1997. Optimization of the design of a multiple-photon excitation laser scanning fluorescence imaging system. *In* Three Dimensional Microscopy: Image Acquisition and Processing IV. *Proc. SPIE*. 2984:25–29.

Yuste, R., and W. Denk. 1995. Dendritic spines as basic functional units of neuronal integration. *Nature*. 375:682–684.